ASTRONOMY & ASTROPHYSICS
SUPPLEMENT SERIES

Astron. Astrophys. Suppl. Ser. **133**, 171–179 (1998)

The Marseille Schmidt survey⋆ for active star-forming galaxies⋆⋆

I. Data on 92 emission line objects in two fields

C. Surace[1,2] **and G. Comte**[2]

[1] Max Planck Institut für Astronomie, Königstuhl 17, D-69117 Heidelberg, Germany
e-mail: surace@mpia-hd.mpg.de
[2] Observatoire de Marseille et Institut Gassendi, 2 place Le Verrier, 13248 Marseille, France

Received February 11; accepted June 4, 1998

Abstract. We present data from a moderately deep spectroscopic Schmidt survey ($B_{\rm lim} = 17.5$) of "active galaxies" selected by the presence of emission lines in their spectra and/or their UV excess. The redshift, magnitudes, color and diameter reduction methods have been discussed in a previous paper. Here we explain the emission line equivalent width determination method.

92 emission line objects have been found in two adjacent fields (approximately $50\,\deg^2$) in the direction of the southern extension of the Virgo cluster. We give a catalog containing positions, photographic R and B magnitudes, $U-R$ colors, effective diameters, redshifts, equivalent widths and intensity ratios of the [OIII]$\lambda\lambda$4959, 5007, H_β and [OII]λ3727 emission lines. On these fields, we evaluate the completeness limit of the survey at a pseudo B magnitude value of 15.7.

A more elaborate astrophysical analysis will appear in a forthcoming paper.

Key words: surveys — galaxies: general — galaxies: starburst — methods: data analysis

1. Introduction

It is expected that, in a nearby future, extragalactic photographic Schmidt surveys will be superseded by CCD-based observations that will go much deeper and are free from the well-known caveats of photographic emulsions. However the giant CCD mosaic detectors that are needed to cover a field of several square degrees are either just beginning operations or still under development. Further, the technical problem due to the field curvature of Schmidt telescopes have prevented the complete coverage of their field with CCDs and lead to build special telescopes based on different optical designs dedicated to CCD wide-field imaging. Therefore, several groups in the recent years have pursued efforts on classical photographic surveys, still fairly well adapted to the statistical study of the galaxian population in the nearby Universe, especially in the field of active galaxy search. Aside from continuing surveys begun long ago and producing large numbers of objects in very homogeneous data bases, such as the Case survey (Pesch & Sanduleak 1983) or the Kiso survey (Takase & Miyauchi-Isobe 1984), other attempts have been directed to a more complete retrieval of the information content of the Schmidt plates, thanks to the capabilities of modern digitization machines and subsequent digital image processing systems. The UC Madrid survey (Zamorano et al. 1994; Gallego et al. 1995), the Montreal Blue Galaxy survey (Coziol et al. 1993, 1994), and the Hamburg Schmidt survey (Hopp et al. 1995; Popescu et al. 1996) are examples of these improvements that enable to go beyond the information content of previous catalogs.

Except for far-infrared selected samples, the search for active galaxies with conventional ground-based telescopes has always been inspired by two basic ideas: to search for emission line spectra or to search for an ultraviolet excess in the continuum of the objects. The two major facets of "activity" in a galaxy are the non-thermal Seyfert-like nuclear phenomena and the enhanced stellar formation producing massive ionizing and rich hot main-sequence stars. They are known to produce *uv*-excess, or at least enhanced blue color, and emission lines. However, the emission lines could be of small equivalent widths in an active object, and therefore very difficult to detect. For instance if the

Send offprint requests to: C. Surace

⋆ The table is also available in electronic form at the CDS via anonymous ftp to cdsarc.u-strasbg.fr (130.79.128.5) or via http://cdsweb.u-strasbg.fr/Abstract.html

⋆⋆ Finding charts, including information on star formation location is available in electronic form via http://www.edpsciences.com

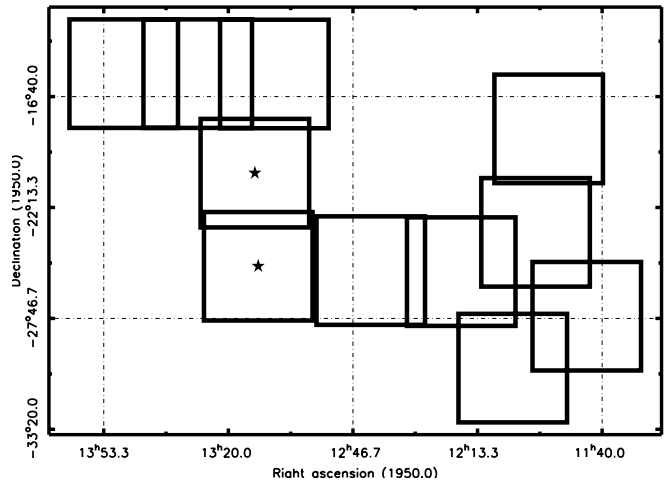

Fig. 1. Configuration of the observed Schmidt plates. The fields used in this study are identified by a central star

star formation burst is seen in an evolved state most of the ionizing fraction of the newborn population has already disappeared. An ideal survey aimed at detecting the totality of the active galaxy population should therefore search for emission lines (including Hα, which in some objects is the only line with substantial equivalent width in the visible), search for ultraviolet excess in the continuum, and be carefully cross-correlated with a deep far-infrared survey to add the dusty objects that escape detection in the visible because of considerable extinction of the active areas.

As a first step to build a sample of "Starburst Galaxies" as complete as possible without constraints either on the morphology or on the cause and/or age of the starburst phenomenon, we have conducted a Schmidt photographic survey using the two modes of selection: ultraviolet excess and emission lines (as for the 2nd Byurakan: Markarian & Stepanian 1983 and Case surveys: Pesch & Sanduleak 1983; Salzer et al. 1995). This allows us to get galaxies experiencing a recent and strong starburst as well as those showing an old dying burst. One of the aim was to get the maximum astrophysical information output directly from the Schmidt plates without any CCD follow-up. For that purpose we have developed specific procedures to process the digitized plates (Surace & Comte 1994, hereafter referred as Paper I).

The present paper focusses on the part of the data reduction not discussed in Paper I (determination of spectrophotometric parameters from the Schmidt photographic low-resolution spectra), an estimate of the completeness of the spectroscopic survey on 2 fields (46.5 square degrees) and contains a catalog of the 92 emission line objects found in these two fields.

2. Observations and digitization

The observational strategies, digitization technique and methods used to retrieve the redshifts, magnitudes, colors and diameters on an homogeneous system are discussed in Paper I. Let us briefly remind that we used the ESO 1 meter Schmidt telescope with and without objective prism (O.P.), taking 3 plates for each field: two O.P. plates on Kodak IIIaJ emulsion, and one bicolor direct plate (U and R exposures separated by 30 arcsec on the same Kodak IIIaF plate). This allows a limiting magnitude on point sources of $B = 17.5$ on O.P. plates and $R = 19.5$ for bicolor plates. The selection of candidate active galaxies is based on the visual evaluation of the ultraviolet excess of the object on the bicolor plate and/or the presence of at least one emission line in its O.P. spectrum. The IIIaJ emulsion allows to study the spectra of the objects in the range 3600 Å – 5330 Å. Thus, the spectral features used to select the active objects are [OIII]$\lambda\lambda$4959, 5007, H_β and [OII]λ3728 emission lines up to a limiting reshift $z = 0.065$. Meanwhile some objetcs can be detected at further redshift using only the [OII] line. After eye selection of candidate targets using binocular microscope, parts of the plates ($10' \times 10'$ or $20' \times 20'$) centered on the objects are digitized by the MAMA (Machine A Mesurer pour l'Astronomie) machine of the Observatoire de Paris. (For a description of the MAMA machine see Guibert et al. 1984; Berger et al. 1991; Guibert & Moreau 1991; Soubiran 1992) O.P. plates were doubled in order to avoid false detections and coadded to improve the signal to noise ratio (cf. Paper I).

11 fields covering a total sky area of some 200 square degrees have been observed in the years 1989-1991 (Fig. 1). This paper deals with the emission line extragalactic objects (hereafter ELGs) found in two adjacent fields in the direction of the South extension of the Virgo Cluster:

$\alpha = 13^{\rm h}12^{\rm mn}00^{\rm s}$, $\delta = -20°30'00''$, and
$\alpha = 13^{\rm h}12^{\rm mn}53^{\rm s}$, $\delta = -25°10'05''$ (equinox 1950).

3. Data reduction

In order to avoid, at least for statistical studies, the difficult long-term task of follow-up observations we have built a reduction system based on automatic procedures using MIDAS imaging package developped at ESO (Fig. 2).

We suggest the reader to refer to Paper I for a complete description of the calibrations, redshift determination technique and photometric measurements. We remind that we succeeded in deriving redshifts with an average accuracy of 160 km s^{-1}, U and R asymptotic magnitudes in Johnson-Cousins system and $U-R$ colors in the Basel system with a mean uncertainty of 0.3 mag. In what follows, we describe the additional data reduction processes used to derive equivalent widths and relative line intensities from the digitized O.P. plates.

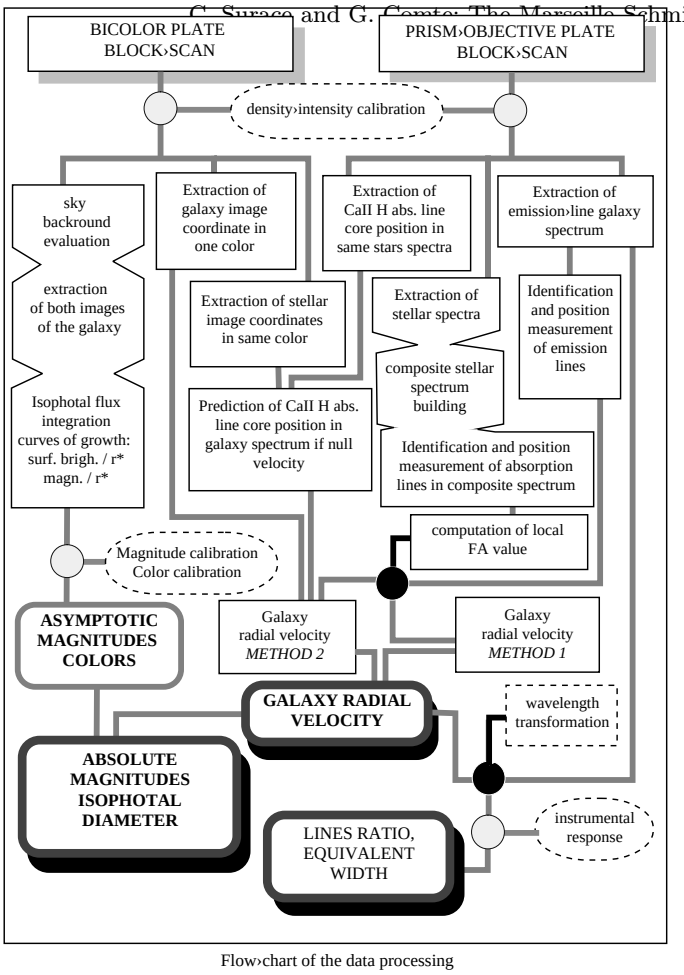

Flow›chart of the data processing

Fig. 2. Flow chart of the data processing. Large black filled circles show internal calibrations while large grey filled circles show calibrations using external objects (spot sensitometer, standard stars, catalogued galaxies)

To perform spectrophotometry on the O.P. spectra of the ELGs, two preliminary steps are needed: the wavelength calibration and derivation of the instrumental response. Figure 2 displays the complete flow chart of the data processing.

3.1. Wavelength transformation

Wavelength calibration of slitless spectra present special difficulties: the absence of calibration lamp spectra or night sky emission line features forbids the use of standard methods designed for slit spectroscopy. The crucial point is to determine some reference wavelength as a reference *position*, in the galaxy spectrum itself. As in Paper I the CaII H 3968 Å absorption line core, was found to be the best reference because of its almost constant presence and good signal-to-noise in the field stars spectra, these field stars being supposed to have an average null radial velocity.

We use the Eq. (2) of Paper I for the CaII H line core. This equation gives the position that the CaII H absorption line core would occupy at null recession velocity in the spectrum of the galaxy using the position of the CaII H absorption line of field stars whose spectra are located in its immediate vicinity.

The equation leads to:

$$X_{\rm o}(\lambda) = X_{\rm G} + \Delta_{\rm Ca} \quad (1)$$

where:

$X_{\rm o}$ is the position that the CaII H absorption line core would occupy in the galaxy spectrum at null recession velocity,

$X_{\rm G}$ is the position of the centroid of the galaxy R image on the bicolor plate,

$\Delta_{\rm Ca}$ is the average separation along the dispersion direction between the field star R positions on the bicolor plate and the CaII H line core position in their respective spectrum. The origin of the coordinates is arbitrary.

From this reference wavelength and solving the equation:

$$|n_{\lambda_2} - n_{\lambda_1}| = \frac{\Delta X}{f \cdot A} \quad (2)$$

where:

ΔX is the separation of two spectral lines along the direction of the prism dispersion, $f \cdot A$, calibrated as described in Paper I, is the product of the focal length of the telescope by the O.P. angle (we remind that we need only to know the *local* value of this product), n_{λ_i} is the prism refractive index for the wavelength λ_i, one can derive the wavelength of any spectral feature from the spatial separation of this feature from the reference position of the CaII H line. Indeed the value of n_{λ_i} depends only on λ_i. It can be calulated with an accuracy of 10^{-5}, using a polynomial approximation given in Schott technical notices for the UBK7 material of the prism.

We used Eqs. (1) and (2) to rescale the spectra along a wavelength scale using a non linear rebinning algorithm.

Tests experienced with the field stars show that the mean error is less than the intrinsic uncertainty in measuring the emission or absorption line (basically ≤ 0.4 Å when measuring Hγ).

To check the internal consistency of the wavelength transformation we derived the redshifts of the objects from the rebinned spectra, and compared them to the values obtained from the methods detailed in Paper I (Fig. 3).

We found the wavelength transformation 95% confident considering all spectra (100% is obtained when the difference between each couple of measured recession velocities, for all the objects, are smaller than 1.5 times the intrinsic uncertainty on the adopted velocity value). This confidence level reaches 100% when only taking into account the spectra with a signal to noise ratio larger than 7. (the S/N ratio being defined as the ratio between the peak intensity of the [OIII]λ5007 Å line and two times the σ value of the noise measured on the continuum between 4400 Å and 4800 Å).

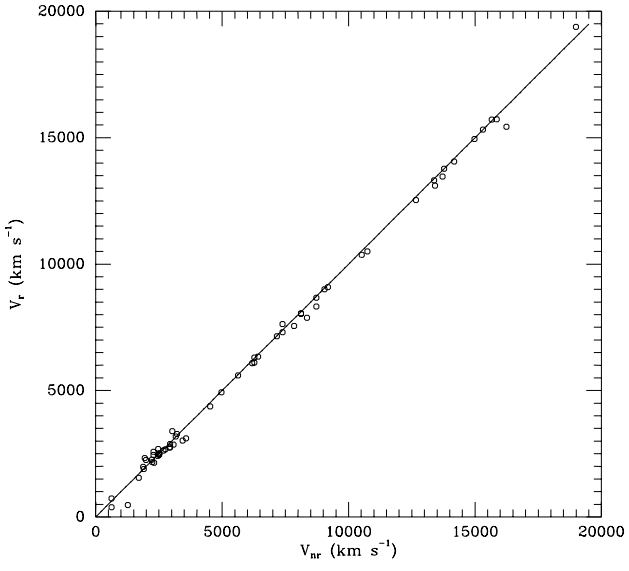

Fig. 3. Comparison of the apparent recession velocities derived from wavelength rebinned spectra (V_r) with the apparent recession velocities adopted from Paper I (V_nr)

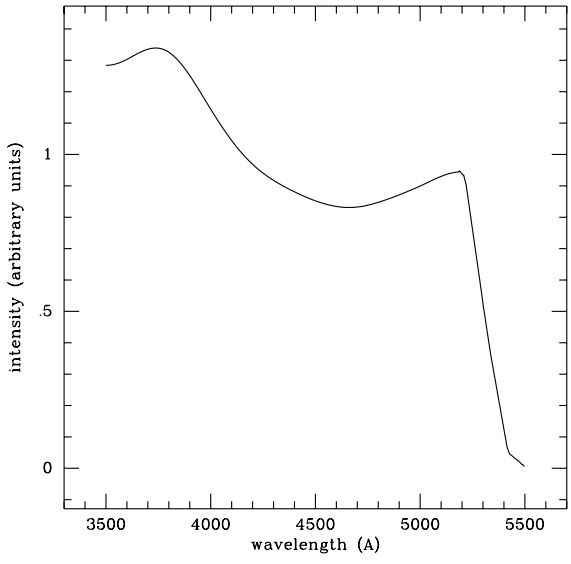

Fig. 4. Telescope-emulsion instrumental response, normalized to 1 at 5200 Å

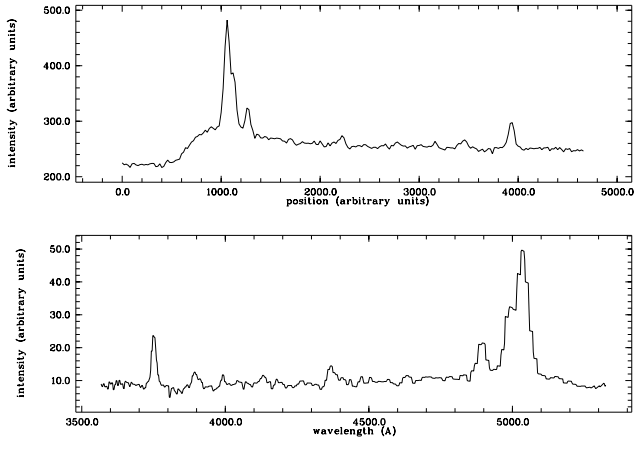

Fig. 5. Up: one dimension galaxy spectrum (13228-1955a) as extracted from the digitized O.P. plate; down: same spectrum, rebinned, and corrected from the instrumental response. The bottom spectrum shows from left to right, [OII] line and Hβ - [OIII] triplet. Hγ, Hδ and [NeIII] are also detected

3.2. Instrumental response

We used the A type field stars, which are easily recognized thanks to the presence of the Balmer absorption lines, to correct the rebinned spectra from the telescope-emulsion instrumental response, as follows. A serie of A-type stars with good signal-to-noise spectra is identified on the O.P. plate and their spectra are digitized in the same conditions as the galaxy spectra, calibrated and rebinned in wavelength, and corrected from the airmass using standard La Silla values of the extinction. However, we do not have at our disposal a series of spectra of spectrophotometric *standard* stars taken with the same instrument. Therefore, we decided to build an "average" spectrum for each subtype $A2V$, $A3V$, $A5V$ and $A7V$, by means of adding individual spectra of several stars of each type. This average spectrum was further normalized at a continuum intensity of 1 at 5200 Å. The instrumental response is obtained by comparing the averaged stellar spectra with those, of same stellar type, observed by Jacobi et al. (1984) and normalized in the same way. The 4 curves obtained by this way are very similar ($\sigma = 0.05$) and are used to derive a mean instrumental response shown in Fig. 4.

The rebinned galaxy spectra are hence divided by the instrumental response to produce the final corrected spectra (Fig. 5).

One can notice the very abrupt drop of the IIIaJ emulsion sensitivity at wavelengths larger than 5200 Å. This well-known characteristic of the IIIaJ emulsion allows to avoid the bright 5577 Å nightsky emission line when making deep photographic imaging but makes spectrophotometry in this spectral region very unsafe, and produces a very large numeric noise on the corrected spectra. A number of ELGs in our sample have a redshift value that pushes the [OIII]λ5007 line in this spectral region. An additional correction has been devised for these galaxies and is described below.

3.3. Measurement of the emission line fluxes and equivalent widths

After rebinning and correction of the spectra from the instrumental response, the ranges where emission lines are present have been selected. Locally, these spectral

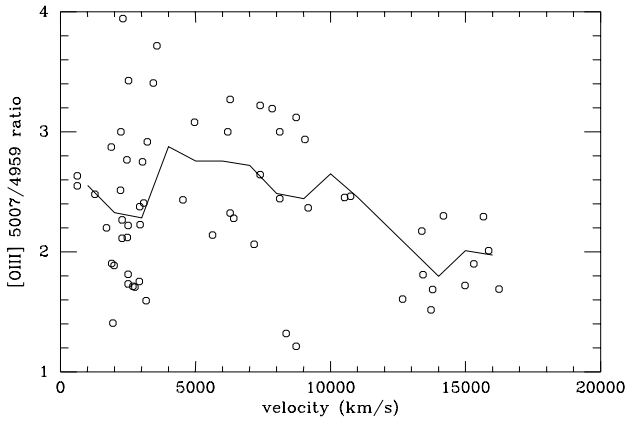

Fig. 6. Dependance [OIII] $\lambda5007/\lambda4959$ ratio on the velocities. The line relies the mean [OIII] ratio value every 1000 km s^{-1}

fractions have been fitted with the addition of a third order polynomial representing the continuum with one or several Gaussians representing the emission lines. The fit used the standard least-squares optimization methods of the MIDAS processing package (associated with NAG mathematical subroutine library). This method used by Cananzi (1993) for the Hβ and Hγ absorption lines, allows a reliable determination of fluxes and equivalent widths, especially for low signal to noise ratio spectra. The line intensity ratios relative to Hβ and equivalent widths of Hβ, [OIII]$\lambda\lambda5007, 4959$ and [OII]$\lambda3728$ emision features were subsequently determined from the Gaussian fits.

From the sample of 92 objects, velocities of which were computed, we measured the R magnitude, $U-R$ color for 66 of them and derived at least one emission line relative flux for 79 of them.

3.4. Intensity correction of the [OIII] lines at high velocities

For velocities larger than 12000 km s^{-1}, the [OIII] doublet enters in the range of sensitivity drop of the IIIaJ emulsion. In this region, the [OIII]$\lambda5007$/[OIII]$\lambda4959$ ratio tends to decrease with velocity, even after instrumental response correction.

The average value of the [OIII] ratio, equal to 2.3 is low with respect to the expected value of 3 given by the theory and is mainly due to the weight of objects with velocities larger than 10000 km s^{-1} (Fig. 6).

In order to use the [OIII] line intensity (and especially the [OIII]/Hβ intensity ratio) for further studies, we have corrected these values using a method of two dimensional mapping. The evolution of the [OIII]$\lambda5007$/[OIII]$\lambda4959$ ratio versus redshift and signal to noise has been mapped from the subsample of 64 galaxies having an [OIII] line measurement. The resulting two-dimension surface has been smoothed and extrapolated across the range:

$0. \leq$ velocity ≤ 25000 km s^{-1} $- \; 0. \leq S/N \leq 20.$

using the following conditions:

$\frac{[\mathrm{OIII}]\lambda5007}{[\mathrm{OIII}]\lambda4959} = 3.$ for $\frac{S}{N} = 20.$ and $vel = 0$ km s^{-1}

and

$\frac{[\mathrm{OIII}]\lambda5007}{[\mathrm{OIII}]\lambda4959} = 0.$ for $\frac{S}{N} = 0.$ and $vel = 25000$ km s^{-1}.

The limiting value equal to 3. is given by the probabilities of transition for the oxygen ion (Osterbrock 1989). The values of the [OIII] lines intensity have subsequently been corrected using this map. The [OIII] doublet intensity ratio corrected in this way has an average value of 3.1 with a standard deviation ($\sigma = 0.71$) identical to that obtained with uncorrected values for objects with velocities smaller than 10000 km s^{-1}.

4. Completeness of the survey

As initially pointed out by Salzer (1989), the completeness of a spectroscopic survey cannot be only derived using the continuum flux of the objects, because an emission line selected sample is not an apparent magnitude limited sample. Indeed because a galaxy is detected by the presence of emission lines in its spectrum, the contrast between the continuum and at least one emission line must be strong enough. That means that a galaxy, the continuum of which is almost invisible against the background intensity, can be selected by the presence of emission line features. On the other hand, the case of an overluminous continuum with weak emission lines could affect the detection of an object only if the level of the continuum is close to the saturation level. This case does not occur in the present study since, thanks to the relatively high dispersion provided by the 4 degrees objective prism of the ESO Schmidt, we are always far from the saturation limit. The eye selection of the emission features remains quite comfortable, even in the spectra of high brightness objects.

Therefore, as shown by Salzer (1989); Salzer et al. (1995); Gallego et al. (1996), one must take into account the value of both continuum and flux of the brightest emission line to derive the completeness of the sample.

We computed an arbitrary magnitude m_{exp} taking into account the continuum flux between 3900 Å and 4980 Å and the flux emitted in the brightest emission line (usually [OIII]$\lambda5007$). This wavelength range used for the continuum flux integration corresponds to a pseudo Johnson B filter. For moderately excited objects at low redshift, the Hβ line is the only significant emission line that could affect the "continuum integration" and its contribution remains moderate. For a few high ionization objects of low redshift, the m_{exp} value will be subject to a significant error due to the emission line contribution in the 3900 Å

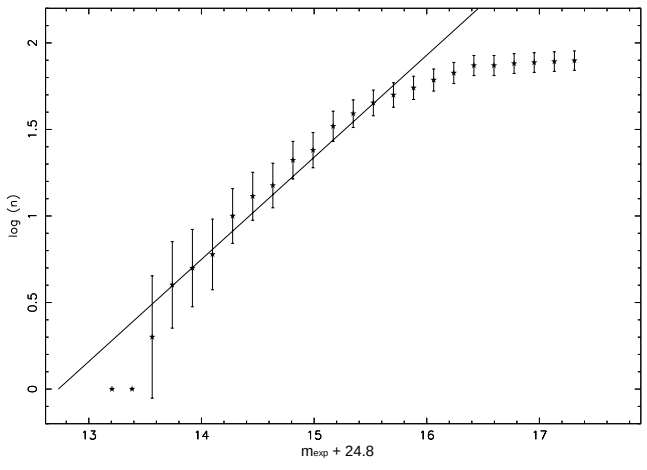

Fig. 7. Plot of the cumulative number of galaxies with apparent magnitude less than $m_{\rm exp}$ versus $m_{\rm exp}$. The line is the result expected for an uniformly distributed sample

and 4980 Å range. Note however that a classical B filter photometry would be subject to the same kind of error.

We do not include in this part of the study the large angular diameter galaxies whose HII regions appear as emission line objects. Using slitless spectroscopy implies an overlapping of several regions from a same object. The wavelength transformation is impossible to compute and hence the continuum flux of these objects cannot be measured. Because these galaxies are bright this will only affect the brightest part of the magnitude distribution, where statistical noise is very large.

The zero point of the $m_{\rm exp}$ magnitude scale has been computed from a comparison with Johnson B apparent magnitudes from the literature for 18 galaxies. We derive the following relation:

$$(m_B)_{\rm lit} = m_{\rm exp} + 24.8\,(\pm 0.3).$$

As a first attempt to determine the completeness of the survey we plotted the logarithm of the cumulative number of galaxies with apparent magnitudes smaller than $m_{\rm exp}$ against $m_{\rm exp}$ and fitted a line of slope 0.6 (assuming that the objects are uniformly distributed in an Euclidean Universe: Mihalas & Binney 1981). The completeness limit is given at the value when the line does not fit anymore the cumulative curve (Fig. 7).

This method uses the same hypothesis as the well-known $V/V_{\rm vmax}$ method (Schmidt 1968) but minimizes the effect of local inhomogeneities (Salzer et al. 1995). From Fig. 7, the present subsample may be considered as complete for $m_{\rm exp} = 15.7$ with 55 objects and a projected density of 1.2 galaxies per square degree. Meanwhile this large value is obtained over a 46.5 square degrees area covering the south extension of the Virgo Supercluster. This large structure should have a density contrast not larger than 3 over the average density observed in the nearby Universe. Therefore, one cannot generalize this result (that can be due to spatial inhomogeneity of the galaxy distribution) to the entire survey.

5. The catalog of the emission line objects

Table 1. Lists the observed objects and presents the following entries:

(1) : number
(2) : identification in standard IAU notation
(3) : previous identification
CTS: Calan-Tololo Survey III (Maza et al. 1991)
NPM: NPM1G. Lick Northern Proper Motion Program (Klemola et al. 1987)
ESO: ESO/Uppsala Survey of the ESO(B) Atlas (Lauberts 1982)
I: IRAS catalog, 1988, Point Sources Catalog
IF: IRAS catalog, 1990, Faint Sources Catalog
HB: Hewitt & Burbige (1991)
(4) : Right ascension (1950.0) (h, mn, s)
(5) : Declination (1950.0) (°, ′, ″)
(6) : Apparent heliocentric velocity (km s^{-1}) (measured and averaged as described in Paper I)
(7) : Uncertainty (km s^{-1})
(8) : Morphology
based on the direct bicolor images and the aspect of the spectrum
Irr: Irregular galaxy; cl.: "clumpy" irregular
HIIr: HII regions in an apparently normal spiral
Sp: Spirals (including galaxies with starburst nuclei)
AGN: Active Galactic Nucleus: Seyfert 1 (Sy1) and Seyfert 2 (Sy2))
LSB: Low Surface Brightness
IP: Interactive pairs
?: unclassified
B: barred object
BC: blue compact galaxy
(9) : R (Cousins) apparent magnitude
based on the images extracted from the direct plates and calibrated as described in Paper I
(10) : R absolute magnitude
assuming $H_0 = 75$ km s^{-1} Mpc^{-1}
(11) : $U-R$ color
derived from the direct bicolor plates, in Basel system (see Paper I)
(12) : Asymptotic Blue apparent magnitude
derived from Blue ESO-SRC Sky Survey plate existing at the Observatoire de Paris. The J plates have been digitized with the MAMA machine using similar procedures as those described in Paper I for our bicolor plates and surface photometry has been performed on the

images. The calibration of the magnitude scale into B magnitudes has been done using published NED or LEDA B magnitudes. The mean error value is similar to that estimated for the R magnitude value (0.3 mag) the * indicates the galaxies used for the calibration

(13) : [OIII]$\lambda\lambda$5007, 4959 equivalent width (in Å)

(14) : Hβ equivalent width (in Å)

(15) : [OII]λ3728 equivalent width (in Å)

(16) : [OIII]λ5007/Hβ observed intensity ratio

(17) : [OII]λ3728/[OIII]λ5007 observed intensity ratio

(18) : Effective diameter (in kpc) assuming $H_0 = 75$ km s^{-1} Mpc^{-1} and equal to twice the effective radius for R images (defined in Paper I).

The plates displayed show the selected galaxies. The target is at the center of the charts surrounded by a circle. if several emission line regions of the same object have been detected, these regions are marked by a diamond. The size of the diamonds is comparable to the size of the emission line region.

If several emission line objects have been detected in the same area, but are not analysed due to the low signal to noise ratio, these objects are marked by a square.

Further papers on this survey will deal with the population of the color–selected galaxies that do not show emission line on the OP plates and on various astrophysical conclusions regarding the total galaxian content of the survey. Characteristics of the objects derived from line ratios and colors will be discussed in a forthcoming paper.

Acknowledgements. C.S. would like to thank Y. Terzian for welcoming at Cornell University and providing all the necessary facilities to write and to finish this paper. C.S would also like to thank R. Giovanelli, M. Haynes for useful remarks and comments.

This research has made use of the NASA/IPAC Extragalactic Database (NED) which is operated by the Jet Propulsion Laboratory, California Institute of Technology, under contract with the National Aeronautics and Space Administration. We have made use of the Lyon-Meudon Extragalactic Database (LEDA) supplied by the LEDA team at the CRAL-Observatoire de Lyon (France)

References

Alonso-Herrero A., Aragon-Salamanca A., Zamorano J., Rego M., 1996, MNRAS 278, 417

Augarde R., Chalabaev A., Comte G., Kunth D., Maehara H., 1994, A&AS 104, 259

Berger J., Cordoni J.P., Fringan A.M., Guibert J., Moreau O., Reboul H., Vanderriest C., 1991, A&AS 28, 377

Cananzi K., 1993, PhD thesis, Observatoire de Marseille

Comte G., Augarde R., Chalabaev A., Kunth D., Maehara H., 1994, A&A 309, 345

Coziol R., Demers S., Pena M., Torres-Peimbert S., Fontaine G., Wesemael F., Lamontagne R., 1993, MNRAS 261, 170C

Coziol R., Demers S., Pena M., Barneoud R., 1994, AJ 108 405C

Jacoby G.H., Hunter D.A., Christian C.A., 1984, ApJS 56, 257

Gallego J., Zamorano J., Aragon-Salamanca A., Rego M., 1995, ApJ 455, 1

Gallego J., Zamorano J., Rego M., Vitores A.G., 1996, A&AS 120, 323

Giovanelli R., Haynes M.P., 1991, ARA&A 29, 499

Guibert J., Charvin P., Stoclet P., 1984, in: Astronomy with Schmidt Type Telescopes, Cappacioli M. (eds.). Reidel p. 165

Guibert J., Moreau O., 1991, ESO Mesenger 64, 69

Haro G., 1956, Bol. obs. Tonantzitla y Tacubaya 14, 329

Hewitt A., Burbidge G., 1991, ApJS 75, 297

Hopp U., Kuhn B., Thiele U., Birkle K., Elsasser H., Kovachev B., 1995, A&AS 109, 537

Klemola A.R., Jones B.F., Hanson R.B., 1987, AJ 94, 501

Lauberts A., the ESO/Uppsala Survey of the ESO(B) Atlas, 1982 ESO

Markarian B.E., 1967, Astrofizika 3, 55

Markarian B.E., Stepanian D.A., 1983, Astrofizika 19, 639

Maza J., Ruiz M.T. Gonzalez L.E., Wischnjewsky M., 1991, A&AS 89, 389

Mihalas D., Binney J., 1981, Galactic Astronomy, 2nd Ed, Freeman

Osterbrock D., 1989, in: "Astrophics of Gaseous Nebulae and Active Galactic Nuclei", Kelly A. (ed.). University Sciences book

Pesch P., Sanduleak R., 1983, ApJS 51, 171

Popescu C., Hopp U., Hagen H.J., Elsässer H., 1996, A&AS 116, 43

Salzer J.J., 1989, ApJ 347, 152

Salzer J.J., Moody J.W., Rosenberg J.L., Gregory S.A., Newberry M.V., 1995, AJ 109, 2376

Schmidt M., 1968, ApJ 151, 393

Soubiran C., 1992, A&A 259, 394

Surace C., 1993, PhD thesis

Surace C., Comte G., 1994, A&A 281, 653 (Paper I)

Takase B., Miyauchi-Isobe N., 1984, Annals Tokyo Astr. Obs. 2nd Ser. XVIII, 55

Zamorano J., Rego M., Gallego J., Vitores A.G., Gonzalez-Riestra R., Rodriguez-Caderot G., 1994, ApJS 95, 387

Zwicky F., 1965, ApJ 142, 1293

Table 1.

(1) n	(2) name	(3) ident	(4) α (1950)	(5) δ	(6) H_{vel}	(7) δv	(8) morph	(9) m_R	(10) R	(11) U-R	(12) m_B	(13) w_{OIII}	(14) $w_{H\beta}$	(15) w_{OII}	(16) $\frac{[OIII]}{H\beta}$	(17) $\frac{[OII]}{[OIII]}$	(18) D_{eff}
1	13016-2236		13 1 34.0	-22 36 55	2886	48	BC	17.0	-15.9	1.7	18.0	85		551		0.60	0.95
2	13020-1850		13 2 2.5	-18 50 56	13386	173	Sp	15.4	-20.9	1.9	17.0	36	9	19	4.10	0.21	8.30
3	13021-2342		13 2 8.7	-23 42 58	6656	70	BC	17.0	-17.7	3.4	18.2						2.07
4	13024-1956a		13 2 25.5	-19 56 10	11079	311	?	17.7	-18.2	2.2	18.7						4.21
5	13024-1956b		13 2 22.0	-19 56 30	7411	246	Irr/Sp	16.2	-18.8	2.1	17.1						4.83
6	13024-1956c		13 2 22.5	-19 56 32	7194	247	companion	18.1	-16.8	2.1	19.0						2.17
7	13026-2228		13 2 36.6	-22 28 55	15098	451	Sp?	16.0	-20.5	2.4	17.4						7.81
8	13027-2314		13 2 43.7	-23 14 2	3213	100	BC	16.0	-17.2	1.8	17.5	322		46	7.58		1.31
9	13034-2221	CTS 1029	13 3 23.5	-22 21 18	10515	100	?	17.2	-18.5	1.9	18.4	64	98	216	0.86	0.74	3.15
10	13036-2118		13 3 37.5	-21 18 30	12666	122	Irr?	15.9	-20.2	1.9	17.0	29	15	45	1.87	0.92	8.51
11	13036-2242	NPM-22.0244	13 3 37.8	-22 42 44	2906	42	BC	15.4	-17.6	2.4	16.5 *	68	13	46	5.11	0.31	1.50
12	13040-2211	ESO 575-055	13 3 58.4	-22 11 19	2543	191	Sp	14.6	-18.1	2.4	16.0 *						1.53
13	13042-2234	ESO 508-04	13 4 10.5	-22 34 23	2725	176	Sp/IP				15.1						
14	13044-2324	NGC4968	13 4 24.1	-23 24 34	3042	217	Sp/AGN	13.0	-20.0	3.4	13.7 *	46					3.29
15	13044-2021		13 4 25.1	-20 21 46	13850	488	Sp/AGN?				18.7						
16	13046-2600		13 4 36.9	-26 0 9	14464	49	Sp/AGN?	17.1	-19.4	1.8	17.8						6.80
17	13050-2631		13 4 57.3	-26 31 0	13202	36	Sp	16.3	-19.9	1.8	17.4						5.16
18	13051-2235	ESO508-11	13 5 3.1	-22 35 25	2659	34	Sp				13.8 *	160	39	282	4.50	0.19	
19	13056-1840		13 5 38.9	-18 40 41	14189	70	BC	16.3	-20.1	1.9	17.5	127		50		0.27	4.75
20	13058-2033		13 5 48.7	-20 33 27	580	112	Irr	15.6	-13.9	2.1	16.8						0.28
21	13060-2406	I13059-2407	13 5 59.6	-24 6 59	4019	100	SY2/Sp	14.6	-19.0	2.9	16.2 *						2.56
22	13064-2020		13 6 26.0	-20 20 30	15311	103	?	17.9	-18.7	2.0	19.1	84	37	175	2.43	0.43	3.96
23	13066-2406	ESO 508-15	13 6 36.1	-24 6 53	3001	100	Irr/clump				14.5	45		104		0.36	
24	13072-2358	ESO 508-19	13 7 9.1	-23 58 24	3147	46	Irr/B				14.3 *	46	16	29	2.91	0.30	
25	13073-2626	ESO 508-21	13 7 17.0	-26 26 35	2100	68	Sp/B nucl				16.3 *						
26	13078-2119		13 7 47.3	-21 19 14	7240	139	?				15.7						
27	13079-2128	ESO 576-03	13 7 53.9	-21 28 57	3281	100	Sp/B HIIr				14.0 *	48	14	79	3.57	0.69	
28	13081-2335	ESO 508-24	13 8 3.5	-23 35 59	2725	72	Sp/B nucl				13.7 *						
29	13082-2041	ESO 576-40	13 8 9.5	-20 41 24	11426	65	I.P				16.3 *						
30	13084-2744	ESO 443-80	13 8 24.5	-27 44 33	2214	25	Sp/B				13.8 *	145	30	25	5.51	0.22	
31	13084-1937		13 8 25.4	-19 37 40	13127	180	Sp ?	16.1	-20.1	2.1	17.3						8.03
32	13085-1901		13 8 29.1	-19 1 45	15855	77	?	18.2	-18.5	1.4	29.3	331	77	40	3.54	0.33	4.97
33	13088-2603		13 8 46.4	-26 3 41	9060	36	BC	16.1	-19.4	2.2	17.6						3.57
34	13090-2016		13 9 1.5	-20 16 20	2353	75	Irr/B	14.7	-17.8	2.1	15.6						1.70
35	13095-1919	NPM-19.0446	13 9 27.1	-19 19 19	7082	615	Irr/B	15.8	-19.0	2.1	17.0						3.77
36	13095-2630		13 9 31.1	-26 30 34	9183	23	?	17.1	-18.3	1.7	18.7	265	49	126	5.76	0.23	3.47
37	13098-2530		13 9 47.0	-25 30 0	15550	100	?	17.7	-18.9	2.0	16.2						3.68
38	13098-2501	CTS 0021	13 9 45.2	-25 1 6	19002	373	SY1	16.0	-21.0	2.1	17.5 *		30				6.85
39	13107-1917		13 10 39.1	-19 17 59	10825	113	Sp/B	15.8	-20.0	1.8	16.7						6.34
40	13114-2123	ESO 576-15	13 11 26.5	-21 23 48	3568	41	Sp/B/LSB?				17.2 *	176	107	11	2.35	0.34	
41	13118-2506		13 11 49.4	-25 6 22	7816	24	?	17.1	-17.9	1.7	18.4	204	45	83	4.81	0.18	3.11
42	13120-2037		13 11 58.7	-20 37 38	12404	343	?				17.1						
43	13122-2148		13 12 13.4	-21 48 59	5624	100	Sp				17.1	197	41		4.88		
44	13124-2432		13 12 21.0	-24 32 11	12132	65	Irr/B	16.4	-19.7	1.6	17.0						
45	13124-1913		13 12 22.3	-19 13 28	7933	70	BC	16.0	-19.1	2.0	17.4						2.79
46	13126-2534		13 12 33.0	-25 34 34	13171	63	Sp/Irr/B	17.3	-19.0	1.4	17.7						

Table 1. continued

(1) n	(2) name	(3) ident	(4) α (1950)	(5) δ	(6) H_{vel}	(7) δv	(8) morph	(9) m_R	(10) R	(11) U-R	(12) m_B	(13) w_{OIII}	(14) $w_{H\beta}$	(15) w_{OII}	(16) $\frac{[OIII]}{H\beta}$	(17) $\frac{[OII]}{[OIII]}$	(18) D_{eff}
47	13125-1943		13 12 30.8	-19 43 31	6418	123	BC	17.4	-17.3	2.2	18.8	140	32		4.64		2.70
48	13125-2005a		13 12 32.4	-20 5 50	7642	234	Sp/B/LSB				17.4						
	13125-2005b		13 12 32.8	-20 5 52	8194	94	?										
49	13128-2343	NGC 5042	13 12 47.9	-23 43 12	1352	57	Sp HIIr				12.2 *	482	146	238	5.28	0.18	
50	13136-2617	ESO 508-33	13 13 38.8	-26 17 50	3259	41	Sp/AGN	13.4	-19.8	2.5	15.0 *	6	7	25	0.86	1.97	2.56
51	13137-2420		13 13 44.5	-24 20 23	1581	177	Sp nucl				17.0						
52	13140-2737	ESO 444-02	13 13 59.8	-27 37 21	1693	23	Sp HIIr				15.0 *	158	33	52	5.02	0.25	
53	13141-2449		13 14 8.8	-24 49 21	13705	53	I.P ?	16.0	-20.3	1.7	17.0	77	29	102	2.82	5.87	0.81
54	13156-2112		13 15 38.0	-21 12 31	16117	70	Sp?	15.6	-21.1	3.9	17.3	56					9.24
55	13160-1849	ESO 576-27	13 15 59.8	-18 49 1	3082	70	Sp	13.9	-19.2	2.3	14.7 *	19	15	31	1.30	0.79	3.02
56	13162-2304	I13161-2304	13 16 9.3	-23 4 23	15497	49	Sp/B/LSB	15.2	-20.4	2.9	16.5	27	16	266	1.72	0.74	11.03
57	13162-2045		13 16 13.1	-20 45 30	8655	70	?				18.4						
58	13162-2046a	NGC 5068	13 16 12.1	-20 46 36	504	70	HIIr					951		479	2.36	0.74	
	13162-2046b		13 16 12.1	-20 46 36	800	70	Sp nucl				10.7 *				3.22	0.23	
59	13163-2512		13 16 19.5	-25 12 36	12068	45	?	18.3	-17.8	1.3	18.9						2.36
60	13172-2334		13 17 10.1	-23 34 45	2177	68	Sp	15.4	-16.9	2.1	16.3	83	17	112	5.15	0.42	
61	13173-1943		13 17 18.7	-19 43 36	6262	50	Irr/Sp	15.2	-19.4	2.0	16.3	224	54	41	3.90	0.31	5.57
62	13176-2316	I13176-2316	13 17 38.6	-23 16 45	13784	100	Sp nucl	15.0	-21.3	2.9	16.8	26	68	14	3.66	0.22	8.91
63	13177-2549	ESO 508-51	13 17 44.9	-25 49 24	1981	43	Sp nucl				14.3 *	29	10	25	2.97	0.43	
64	13181-2313	IF13181-2312	13 18 5.9	-23 13 9	1860	42	I.P	15.7	-16.3	1.9	17.0	33	5	77	7.13	0.66	1.43
65	13181-2034		13 18 6.0	-20 34 20	3138	324	?	18.2	-14.9	1.7	18.8						0.97
66	13183-2026		13 18 15.8	-20 26 39	14106	243	Irr ,I.P	15.9	-20.5	2.3	17.2						8.35
67	13194-2214		13 19 24.0	-22 14 21	9074	54	BC	16.6	-18.8	2.3	18.3	59	10	61	6.08	0.44	
68	13191-2212		13 19 6.9	-22 12 51	7164	148	BC	16.4	-18.5	2.3	17.6	30	9	34	2.16	1.01	
69	13192-2513	ESO 508-59	13 19 10.1	-25 13 56	2204	27	Sp/ HIIr				15.1 *	129	16	50	8.38	0.16	
70	13195-2211		13 19 27.5	-22 11 0	9538	147	Sp ?	16.3	-19.2	2.6	18.3						3.65
71	13196-1904		13 19 34.1	-19 4 55	5060	70	LSB/B ?	16.6	-17.6	1.9	17.8						2.80
72	13198-2020		13 19 45.1	-20 20 5	6189	70	Sp/AGN ?	17.5	-17.1	2.0	18.3	230					1.57
73	13206-2535	IF13205-2536	13 20 33.0	-25 35 59	10192	61	Sp/AGN	15.5	-20.2	2.5	17.3						4.96
74	13210-2723	Abell 1736	13 20 59.4	-27 23 58	2388	54	SY2	15.5	-17.0	1.9	17.0 *	25	5	10	4.44	0.32	0.82
75	13211-1926	NPM-19.0448	13 21 7.7	-19 26 10	5305	206	Sp/AGN	16.0	-18.3	2.0	17.0						2.54
76	13214-1934		13 21 24.0	-19 34 48	7788	116	Irr/B?	16.8	-18.3	1.9	17.8						3.55
77	13214-2337	ESO 508-67	13 21 26.2	-23 37 0	7362	38	Sp/I.P	13.9	-21.0	2.4	15.3 *	13	6	2.34	0.84	31	
78	13217-2434		13 21 40.6	-24 34 58	9404	136	?	18.0	-17.5	1.9	18.9						3.25
79	13217-2023		13 21 43.6	-20 23 24	8120	163	?	16.9	-18.3	1.8	18.1	71	11	44	6.54	0.32	
80	13218-2023	NPM-20.0399	13 21 48.0	-20 23 14	8044	90	Sp/AGN?	15.5	-19.6	2.0	16.7						3.69
81	13220-1926	ESO 576-50	13 21 59.5	-19 26 8	2232	100	Sp/B+comp?				13.2 *	3439	75	56	6.51	0.21	
82	13223-2409		13 22 15.7	-24 9 45	1594	31	Irr/Sp	16.2	-15.5	2.2	17.0	38	16	50	2.22	0.46	1.61
83	13225-2614	I13225-2614	13 22 30.6	-26 14 14	18440	51	Sp/Irr	15.6	-21.4	2.0	16.6 *						8.83
84	13228-2540		13 22 48.7	-25 40 0	4523	34	Sp/Irr				17.5	191	40	97	4.80	0.21	
85	13228-1954		13 22 45.9	-19 54 8	8721	141	Irr/sp	15.2	-20.1	2.1	16.7	35	4	27	7.46	0.58	3.80
86	13228-1955	IF13227-1954	13 22 47.6	-19 55 4	8345	90	Irr,I.P	16.0	-19.3	1.9	17.6				5.56	0.24	
87	13228-1954	IF13227-1954	13 22 47.6	-19 54 50	7862	101	Irr,I.P	17.3	-17.8	1.5	16.7				5.83	0.36	
88	13228-2547		13 22 47.6	-25 47 13	4458	70	BC	17.9			17.9	52	5	54	9.55	0.50	
89	13229-2118		13 22 53.0	-21 18 20	8405	70	Irr/B	16.0	-19.3	1.8	16.8	150					4.76
90	13230-1958		13 23 0.7	-19 58 29	2299	119	Irr	15.9	-16.5	2.2	17.0						
91	13232-2322	CTS 1031	13 23 14.4	-23 22 33	13421	85	Sp				18.9	328	78	532	4.84	0.28	
92	13243-2741	ESO 444-39	13 24 19.9	-27 41 49	2023	37	Sp/B	13.6	-18.6	2.2	14.9	190	41	42	4.83	0.15	1.97